Normal mode approach for predicting the mechanical properties of solids from first principles: Application to compressibility and thermal expansion of zeolites

R. Astala,* Scott M. Auerbach,† and P. A. Monson‡
Department of Chemistry and Department of Chemical Engineering, University of Massachusetts, Amherst, Massachusetts 01003, USA
(Received 1 July 2004; revised manuscript received 1 October 2004; published 25 January 2005)

We present a method for analyzing the mechanical properties of solids, based on normal modes and their coupling to lattice strains. This method was used to study elastic compression and thermal expansion of zeolites, with parameters calculated from density functional theory. We find in general that the bulk modulus can be divided into two contributions: a positive term arising from compression without internal relaxation, and a negative term from coupling between compression and internal vibrational modes. For silica polymorphs, the former term varies little among the phases studied, reflecting the intrinsic rigidity of SiO_4 tetrahedra. In contrast, the latter term varies strongly from one polymorph to the next, because each polymorph exhibits different symmetry constraints on internal vibrations and their couplings to lattice strains. Typically only a few normal modes contribute to the bulk modulus. To facilitate parametrization of this normal mode model, we constructed a simplified classical spring-tetrahedron model for silica. After fitting to properties of silica sodalite, this model reproduces cell volumes and predicts bulk moduli of α-cristobalite and silica zeolites CHA, LTA, and MFI. We incorporated anharmonic effects into the theory, allowing the calculation of the thermal expansion coefficient. The resulting expression provides a generalization of classical Grüneisen theory, taking into account additional anharmonicities. This method was used to study thermal expansion of fcc aluminum and an aluminosilica sodalite, yielding good agreement with experiment.

DOI: 10.1103/PhysRevB.71.014112 PACS number(s): 62.20.Dc, 65.40.De, 71.15.Mb, 82.75.−z

I. INTRODUCTION

The discovery of new nanostructures with increasingly complex architectures challenges our understanding of the relationship between a material's atomic structure and its mechanical properties.[1] An important example involves the crystalline polymorphs of silica, SiO_2. These include dense phases such as quartz and cristobalite,[2] as well as nanoporous (zeolitic) polymorphs such as sodalite and silicalite.[3] The mechanical properties of zeolites are particularly important because channel deformations can radically change a zeolite's capacity for adsorption, diffusion, and reaction. These dense and nanoporous phases share common structural features, including Si-O bond lengths ($\sim$1.6 Å), O-Si-O angles ($\sim$109°), and networks with low coordination and strong association.[4] These phases differ in Si-O-Si angles (140°–180°), densities and symmetries. The cohesive energy appears to be relatively insensitive to these structural differences, varying by only 0.1 eV per SiO_2.[5] However, the bulk modulus varies significantly from one polymorph to the next.[5] Despite progress in understanding the mechanical properties of networks,[6] this variation in bulk modulus among silica phases remains poorly understood. In this article, we investigate a theory of solid compression and expansion based on normal vibrations and their coupling to lattice strains, which elucidates the relationship between a crystal's structure and its mechanical properties.

The elastic response of a solid to compression can be decomposed into two parts: (i) atomic vibrations at fixed volume,[7,8] and (ii) unit cell volume fluctuations for a fixed atomic configuration. In what follows, we denote the latter motion as a "sudden" elastic response, because the vibrations do not relax during compression. Our theory begins by writing a classical harmonic potential energy in terms of these two kinds of distortions. Although our classical treatment breaks down at sufficiently low temperatures, where the quantum nature of vibrations becomes important, the bulk modulus turns out to be most sensitive to low-frequency vibrations, which are adequately modeled under ambient conditions by classical theory. Below we show that the bulk modulus can be written as a positive term arising from sudden elastic response, and a negative term controlled by couplings between vibrations and lattice strains. When parametrized for several silica polymorphs by density functional theory (DFT) calculations, we find that the sudden elastic response is remarkably uniform from one polymorph to the next, like the cohesive energy discussed above. However, normal vibrations and their couplings to lattice strain are found to depend sensitively on the symmetry of a given polymorph.

By augmenting the harmonic potential energy with anharmonicity, we have developed a theory for the thermal expansion of crystalline solids. Our approach provides a generalization to classical Grüneisen theory,[9] which accounts for anharmonicity by tracking the volume dependence of phonon frequencies. Instead, we construct a potential with a complete set of cubic anharmonicities, and derive analytically the thermal expansion coefficient showing the importance of each kind of anharmonicity. We apply this approach to the thermal expansion of aluminum metal and aluminosilica sodalite zeolite. In the former case, we find that our theory reproduces the success of classical Grüneisen theory. In the latter case, we find that our approach gives good agreement with experiment, while Grüneisen theory accounts for only 22% of the thermal expansion coefficient.

To facilitate the parametrization of this normal mode potential function, we develop a classical spring-tetrahedron

model for silica. This approach was inspired by rigid-unit models developed by Dove and co-workers to study soft vibrational modes in silica.[10] In our model, SiO_4 units are treated as semirigid tetrahedra, while Si-O-Si angles are relatively flexible. Our spring-tetrahedron model is similar in spirit to valence bond force fields developed for simulating zeolite framework vibrations.[11,12] These force fields were designed to accurately reproduce infrared spectra of zeolites. In contrast, the spring-tetrahedron model was constructed to provide a simple, qualitative picture of zeolite compression. We show below that, despite its simplicity, the spring-tetrahedron model reproduces cell volumes and predicts bulk moduli of several silica phases. In the end we find that the normal mode picture of compression and expansion, parametrized by DFT calculations and the spring-tetrahedron model, provides a powerful new approach for understanding the mechanical properties of nanostructured materials.

The remainder of this paper is organized as follows: in Sec. II we present the normal mode theory of crystalline compression and expansion, deriving equations for the bulk modulus and thermal expansion coefficient. In Sec. III we describe the DFT and spring-tetrahedron calculations required to parametrize the new theory. In Sec. IV we give the results for a variety of materials including several silica polymorphs, aluminum metal, and an aluminosilica sodalite. In Sec. V we discuss our results and offer concluding remarks. Finally, we present an Appendix to clarify our derivation of the bulk modulus for anisotropic crystals.

II. THEORY

Here we present an approach for studying mechanical properties of solids based on classical normal mode analysis. As discussed above, elastic responses are usually dominated by lower frequency vibrations, which are adequately treated with classical theory. The theory presented below is applicable to the mechanical properties of general anisotropic lattices. For pedagogical purposes, we begin by deriving an expression for the bulk modulus in the simple case of a cubic lattice. We then proceed to the more general case of anisotropic lattices. We end this section by deriving an expression for the thermal expansion coefficient for cubic lattices.

A. Harmonic approximation for cubic lattices

The harmonic potential energy of the lattice, E_0, can be expressed in terms of small displacements of the lattice parameter given by $l=a-a_0$, where $V_0=a_0^3$ is the equilibrium unit cell volume at $T=0$ K. The energy also depends on an n-dimensional vector of fractional Cartesian displacements $\mathbf{q}=(\mathbf{r}-\mathbf{r_0})/a$ from an equilibrium geometry $\mathbf{r_0}$. We use fractional coordinates to describe vibrations so that varying the strain l, while keeping $\mathbf{q}$ fixed, produces isotropic compression/expansion of the system. By performing an orthogonal transformation to normal modes $\mathbf{x}=\mathbf{U}^{\mathrm{T}}\mathbf{q}$, we express the harmonic lattice energy according to

$$E_0(x_1,\ldots,x_n,l)=\sum_{i=1}^{n}(D_i x_i^2+L_i x_i l)+Kl^2. \tag{1}$$

Here $\{D_i\}$ are the normal mode force constants, which can be computed by mapping the potential energy, or the forces, for small atomic displacements. This procedure gives a nondiagonal force constant matrix, which is then diagonalized to obtain $\{D_i\}$ and $\mathbf{x}$. The parameter K controls the energy cost of a sudden elastic response, i.e., isotropic expansion or contraction of the solid. The parameters $\{L_i\}$ describe the coupling between normal mode displacements and lattice strain. This kind of potential energy function is a starting point for activated rate theories,[13] and has also been used to study displacive phase transitions in ferroelectric materials within the effective Hamiltonian approach.[14–16]

We note that normal mode analysis applied to small molecules usually involves mass weighting the force constant matrix, which upon diagonalization yields normal mode force constants with units of square frequency.[17] In contrast, we use fractional coordinates and omit the mass weighting for simplicity, so that D_i has units of energy.

The bulk modulus is expressed as

$$B=-V\left(\frac{\partial p}{\partial V}\right)_{n,T}=-V\left(\frac{\partial V}{\partial p}\right)_{n,T}^{-1}=-V\left(\frac{\partial \Delta V}{\partial p}\right)_{n,T}^{-1}, \tag{2}$$

where $\Delta V=V-V_0$ is the volume change relative to the equilibrium volume V_0 at $T=0$ K. Because the energy in Eq. (1) depends explicitly on volume through the strain l, we average over volume fluctuations in the npT ensemble to obtain $\langle V\rangle$ and hence $\langle \Delta V\rangle$, according to

$$\langle \Delta V\rangle=-\frac{\partial}{\beta\partial p}\ln Q(n,p,T)=-\frac{\partial}{\beta\partial p}\ln\int_{-\infty}^{\infty}dx_1\cdots dx_n\,dl \times\exp[-\beta(E_0+p\Delta V)]. \tag{3}$$

In the limit of small strains for cubic lattices, we can substitute $\Delta V\cong 3a_0^2 l$. This approximation, which is consistent with the harmonic energy expression in Eq. (1), leads to a product of Gaussian integrals that can be evaluated successively over normal modes. After one such integration, we obtain

$$\langle \Delta V\rangle=-\frac{\partial}{\beta\partial p}\ln\int_{-\infty}^{\infty}dx_1\cdots dx_{n-1}\,dl \times\exp\left\{-\beta\left[\sum_{i=1}^{n-1}(D_i x_i^2+L_i x_i l)+\left(K-\frac{L_n^2}{4D_n}\right)l^2+p\,\Delta V\right]\right\}. \tag{4}$$

As such, coupling to the nth normal mode effectively reduces the sudden elastic force constant K to $K-L_n^2/4D_n$. After integrating over all degrees of freedom we obtain

$$\langle \Delta V\rangle=-\frac{\partial}{\beta\partial p}\ln\left\{\exp\left[\frac{\beta}{4K'}(3a_0^2 p)^2\right]\right\}, \tag{5}$$

where

$$K'=K-\sum_{i=1}^{n}\frac{L_i^2}{4D_i}. \tag{6}$$

By substituting this result into Eq. (2) and taking the zero pressure limit, we obtain

$$B = \frac{2}{9a_0}K' = \left(\frac{2}{9a_0}K\right) - \left(\frac{2}{9a_0}\sum_{i=1}^{n}\frac{L_i^2}{4D_i}\right) \equiv B_{\mathrm{sud}} - B_{\mathrm{vib}}. \tag{7}$$

Thus, the present theory shows that for cubic lattices, the bulk modulus can be expressed as a sudden elastic response B_{sud} which is softened by an amount B_{vib} through coupling to vibrations. B_{sud} is the bulk modulus in a fictitious situation in which the fractional coordinates of atoms are fixed. Coupling to vibrations softens this response by an amount B_{vib} so that if a normal mode is either floppy, i.e., small D_i, or strongly coupled, i.e., large L_i, it decreases the bulk modulus to a greater extent.

B. Harmonic approximation for anisotropic lattices

Silica polymorphs typically exhibit anisotropic lattices. If there are m independent lattice parameters, e.g., $m=3$ for an orthorhombic cell, the energy expression generalizes to

$$E_0(x_1,\ldots,x_n,l_1,\ldots,l_m) = \sum_{i=1}^{n}\left(D_i x_i^2 + \sum_{j=1}^{m} L_{ij}x_i l_j\right) + \sum_{j,j'=1}^{m} K_{jj'}l_j l_{j'}. \tag{8}$$

These normal modes are obtained from fractional Cartesian displacements whose x, y, and z components are scaled by their respective lattice parameters. In this subsection, the index i runs over vibrational modes, while the indices (j,j') run over lattice parameters. Using Eq. (8) to compute the npT partition function again leads to a product of Gaussian integrals. However, in this case the anisotropic $p\Delta V$ term is slightly more complicated. We again focus on the limit of small volume changes, and define an m-dimensional vector $\mathbf{c}$ so that the volume change takes the form

$$\Delta V = \sum_{j=1}^{m} c_j l_j. \tag{9}$$

For example, the volume of an orthorhombic unit cell is given by

$$V = (a_1 + l_1)(a_2 + l_2)(a_3 + l_3), \tag{10}$$

where (a_1,a_2,a_3) are the $T=0$ K lattice parameters, and (l_1,l_2,l_3) are the anisotropic strains. To lowest order in these strains, the volume change is given by

$$\Delta V = V - V_0 = V - a_1a_2a_3 = a_2a_3l_1 + a_3a_1l_2 + a_1a_2l_3. \tag{11}$$

Comparing Eq. (11) with Eq. (9) suggests that the vector $\mathbf{c}$ is given by $c_1=a_2a_3$, $c_2=a_1a_3$ and $c_3=a_1a_2$. This approach can also be used for systems with nonorthogonal lattice vectors, as long as their angles remain fixed. In such a case, the vector $\mathbf{c}$ depends on the unit cell shape. The evaluation of the multidimensional Gaussian integral is presented in the Appendix. We obtain the following equation for the bulk modulus:

$$B = 2V_0\left(\mathbf{c}^T\mathbf{K}'^{-1}\mathbf{c}\right)^{-1}, \tag{12}$$

where the matrix $\mathbf{K}'$ is defined by

$$K'_{jj'} = K_{jj'} - \sum_{i=1}^{n}\frac{L_{ij}L_{ij'}}{4D_i}. \tag{13}$$

The sudden elastic response for anisotropic systems can be extracted by setting the L_{ij} couplings to zero in Eq. (13), giving $B_{\mathrm{sud}}=2V_0(\mathbf{c}^T\mathbf{K}^{-1}\mathbf{c})^{-1}$. If the system were cubic, i.e., with only one independent lattice parameter, then $\mathbf{K}$, $\mathbf{K}'$, and $\mathbf{c}$ reduce to scalars, and we recover the previous results in Eq. (7).

C. Anharmonic treatment of cubic lattices: Simple case

Silica polymorphs often exhibit low frequency normal modes due to flexible Si-O-Si angles, which give rise to interesting behavior such as negative thermal expansion coefficients.[18,19] Soft mode behavior is encountered in other systems such as ferroelectric materials.[14] To treat such phenomena we consider anharmonic perturbations expressed in normal mode coordinates. In what follows, we consider the thermal expansion of cubic lattices; the generalization to anisotropic systems will be reported in a forthcoming publication. We augment the harmonic energy E_0 with a complete set of third-order anharmonicities. To ensure the convergence of partition functions, we also add fourth-order anharmonicities; the corresponding fourth-order constants are set to zero after integration. For pedagogical purposes, we begin by treating the simple case of only a single uncoupled normal mode. This will turn out to yield a result essentially identical to classical Grüneisen theory.[9] In the next section, we generalize this to the multi-dimensional coupled case for cubic lattices.

The harmonic energy of one normal mode uncoupled from cubic lattice strain is given by $E_0(x,l)=Dx^2+Kl^2$. In this simple case, we augment E_0 with the anharmonicity $\epsilon x^2 l$, and also with fourth-order convergence factors. The energy thus becomes

$$E(x,l) = E_0(x,l) + \epsilon x^2 l + (\lambda^{(x)}x^4 + \lambda^{(l)}l^4). \tag{14}$$

To facilitate evaluating the partition function, we assume that the anharmonic effects are relatively small and expand the anharmonic contribution to the Boltzmann factor to first order, yielding

$$\langle \Delta V\rangle = -\frac{\partial}{\beta\partial p}\ln\int_{-\infty}^{\infty} dx\,dl\,\exp\{-\beta[E_0(x,l)+p\Delta V]\} \times(1-\beta\epsilon x^2 l+\cdots). \tag{15}$$

At this stage the fourth-order terms may be discarded. We add auxiliary terms αx and γl to $E_0+p\Delta V$, which allows us to write the partition function using derivatives of α and γ by applying the Leibniz integration rule according to

$$\langle \Delta V \rangle = -\frac{\partial}{\beta \partial p} \ln \left\{ \left(1 + \beta^{-2} \epsilon \frac{\partial^3}{\partial \alpha^2 \partial \gamma} \right) \int_{-\infty}^{\infty} dx\, dl \times \exp\{-\beta [E_0(x,l) + p\,\Delta V + \alpha x + \gamma l]\} \right\} \Bigg|_{\alpha,\gamma \to 0}. \tag{16}$$

The Gaussian integral can be evaluated as was done for the cubic harmonic case discussed above, leading to

$$\langle \Delta V \rangle = -\frac{\partial}{\beta \partial p} \ln \left\{ \left(1 + \beta^{-2} \epsilon \frac{\partial^3}{\partial \alpha^2 \partial \gamma} \right) \times \exp\left[\frac{\beta}{4K} (3a_0^2 p + \gamma)^2 + \beta \frac{\alpha^2}{4D} \right] \right\} \Bigg|_{\alpha,\gamma \to 0}. \tag{17}$$

Differentiating with respect to α and γ and setting $\alpha = 0 = \gamma$ yields the equation of state:

$$\langle \Delta V \rangle = \left(\frac{-9a_0^4}{2K} \right) p + \left(\frac{-3a_0^2 \epsilon}{4KD} \right) \beta^{-1}. \tag{18}$$

The first term on the right-hand side of Eq. (18) yields the sudden elastic response found above for cubic lattices. The second term gives the thermal expansion coefficient, C, which is defined by

$$C \equiv \frac{1}{V} \left(\frac{\partial V}{\partial T} \right)_{n,p} = \frac{1}{V} \left(\frac{\partial \Delta V}{\partial T} \right)_{n,p}. \tag{19}$$

Evaluating the derivative and setting the normalizing volume to its zero-point value of a_0^3 gives

$$C = \frac{1}{a_0^3} \left(\frac{-3a_0^2 \epsilon k_B}{4KD} \right) = -\left(\frac{3\epsilon k_B}{4a_0 KD} \right), \tag{20}$$

where k_B is Boltzmann's constant. We note that the sign of C is controlled by and opposite to the sign of the anharmonicity parameter, ϵ.

The result in Eq. (20) is analogous to the classical Grüneisen theory of thermal expansion,[9] which can be seen by writing the energy as

$$E(x,l) = (D + \epsilon l)x^2 + Kl^2 + (\lambda^{(x)} x^4 + \lambda^{(l)} l^4). \tag{21}$$

Equation (21) clearly shows how anharmonicity can manifest itself through normal mode frequencies that depend on volume. Indeed, the Grüneisen theory is cast in terms of the parameter γ_G given by

$$\gamma_G = -\frac{V}{\omega} \frac{d\omega}{dV}. \tag{22}$$

Assigning the normal mode an arbitrary mass m leads to

$$\omega = \sqrt{\frac{2(D + \epsilon l)}{m}}, \tag{23}$$

which gives the following Grüneisen parameter:

$$\gamma_G = -\frac{a_0 \epsilon}{6D}. \tag{24}$$

The equation for thermal expansion within Grüneisen theory is given by[9]

$$C = \frac{\gamma_G C_V}{VB}, \tag{25}$$

where C_V is the heat capacity at constant volume. Using the classical Dulong–Petit value $C_V = nk_B$ with $n=1$, and substituting Eq. (7) for the uncoupled bulk modulus $B = 2K/9a_0$, we recover the result in Eq. (20). The fact that we recovered classical Grüneisen theory without coupling between vibration and strain, and with only one of many possible anharmonicities, suggests that a more complete theory of thermal expansion is possible, which we develop below.

D. Anharmonic treatment of cubic lattices: General case

We now consider thermal expansion for a cubic system with n normal modes coupled to strain, and with the complete set of third-order anharmonicities. We find below that the presence of vibrations coupled to strain leads to qualitatively different thermal expansion behavior. The energy now takes the form

$$E(x_1, \ldots, x_n, l) = E_0(x_1, \ldots, x_n, l) + \sum_{i,j,k=1}^{n} \epsilon_{ijk}^{(3)} x_i x_j x_k + \sum_{i,j=1}^{n} \epsilon_{ij}^{(2)} x_i x_j l + \sum_{i=1}^{n} \epsilon_i^{(1)} x_i l^2 + \epsilon^{(0)} l^3 + \left(\sum_{i=1}^{n} \lambda_i^{(x)} x_i^4 + \lambda^{(l)} l^4 \right). \tag{26}$$

Here E_0 is the harmonic potential energy in Eq. (1) with vibrations coupled to strain. Once again, the anharmonic contribution to the Boltzmann factor is expanded to first order, yielding

$$\langle \Delta V \rangle = -\frac{\partial}{\beta \partial p} \ln \int_{-\infty}^{\infty} dx_1 \ldots dx_n\, dl \exp\{-\beta [E_0(x_1, \ldots, x_n, l) + p\Delta V]\} \left(1 - \beta \sum_{i,j,k=1}^{n} \epsilon_{ijk}^{(3)} x_i x_j x_k - \beta \sum_{i,j=1}^{n} \epsilon_{ij}^{(2)} x_i x_j l - \beta \sum_{i=1}^{n} \epsilon_i^{(1)} x_i l^2 - \beta \epsilon^{(0)} l^3 - \cdots \right). \tag{27}$$

The fourth-order terms are included merely as convergence factors for the integral, and can be discarded once the expansion is made. We now add auxiliary terms $\Sigma_{i=1}^{n} \alpha_i x_i$ and γl to the exponential, which again allows us to write the partition function using derivatives according to

$$\langle \Delta V \rangle = -\frac{\partial}{\beta \partial p} \ln\Bigg(1 + \beta^{-2} \sum_{i,j,k=1}^{n} \epsilon_{ijk}^{(3)} \frac{\partial^3}{\partial\alpha_i\, \partial\alpha_j\, \partial\alpha_k} + \beta^{-2} \sum_{i,j=1}^{n} \epsilon_{ij}^{(2)} \frac{\partial^3}{\partial\alpha_i\, \partial\alpha_j\, \partial\gamma} + \beta^{-2} \sum_{i=1}^{n} \epsilon_{i}^{(1)} \frac{\partial^3}{\partial\alpha_i\, \partial\gamma^2} + \beta^{-2} \epsilon^{(0)} \frac{\partial^3}{\partial\gamma^3} \Bigg) \int_{-\infty}^{\infty} dx_1 \cdots dx_n\, dl \times \exp\Bigg\{ -\beta \Bigg[E_0(x_1, \ldots, x_n, l) + p\, \Delta V + \sum_{i=1}^{n} \alpha_i x_i + \gamma l \Bigg] \Bigg\}. \tag{28}$$

After evaluating the Gaussian integrals, we obtain

$$\langle \Delta V \rangle = -\frac{\partial}{\beta \partial p} \ln\Bigg\{ \Bigg(1 + \beta^{-2} \sum_{i,j,k=1}^{n} \epsilon_{ijk}^{(3)} \frac{\partial^3}{\partial\alpha_i\, \partial\alpha_j\, \partial\alpha_k} + \beta^{-2} \sum_{i,j=1}^{n} \epsilon_{ij}^{(2)} \frac{\partial^3}{\partial\alpha_i\, \partial\alpha_j\, \partial\gamma} + \beta^{-2} \sum_{i=1}^{n} \epsilon_{i}^{(1)} \frac{\partial^3}{\partial\alpha_i\, \partial\gamma^2} + \beta^{-2} \epsilon^{(0)} \frac{\partial^3}{\partial\gamma^3} \Bigg) \exp\Bigg[\frac{\beta}{4K'} \Bigg(3a_0^2 p + \gamma - \sum_{i=1}^{n} \frac{L_i}{2D_i} \alpha_i \Bigg)^2 + \beta \sum_{i=1}^{n} \frac{\alpha_i^2}{4D_i} \Bigg] \Bigg\} \Bigg|_{\alpha_i, \gamma \to 0}, \tag{29}$$

where K' is given by Eq. (6). Differentiating with respect to α_i and γ, setting $\alpha_i = 0 = \gamma$, and assuming the limit of low temperature and pressure yields an equation of state of the form $\langle \Delta V \rangle = V_0(-p/B + TC)$, where B is the bulk modulus and C is the thermal expansion coefficient. These manipulations yield the following expression for $\langle \Delta V \rangle$:

$$\langle \Delta V \rangle = -\frac{9a_0^4}{2K'} p - \beta^{-1} \frac{3a_0^2}{4K'} \Bigg(\sum_{i=1}^{n} \frac{\epsilon_{ii}^{(2)}}{D_i} - \sum_{i,j=1}^{n} \frac{3L_j}{2D_j} \frac{\epsilon_{iij}^{(3)}}{D_i} \Bigg) - \beta^{-1} \frac{9a_0^2}{4K'^2} \Bigg(\epsilon^{(0)} - \sum_{i=1}^{n} \epsilon_i^{(1)} \frac{L_i}{2D_i} + \sum_{i,j=1}^{n} \epsilon_{ij}^{(2)} \frac{L_i L_j}{4D_i D_j} - \sum_{i,j,k=1}^{n} \epsilon_{ijk}^{(3)} \frac{L_i L_j L_k}{8D_i D_j D_k} \Bigg). \tag{30}$$

Equation (30) shows that the bulk modulus is not influenced by anharmonicity at this level of theory. The terms proportional to β^{-1} describe thermal expansion, which vanishes in the limit of all $\epsilon \to 0$. This expression is similar to that of the bulk modulus in Eq. (7), in that it contains a "sudden anharmonic" term $\epsilon^{(0)}$ that is corrected by terms arising from coupling between the lattice strain and normal modes. Our numerical calculations below reveal that the various terms in Eq. (30) exhibit different scaling behaviors with system size. In particular, in the limit of large system sizes, i.e. many normal modes, the thermal expansion coefficient becomes dominated by the first two terms proportional to β^{-1}. These terms scale as a_0^3, while the four other terms on the right remain constant. The first term proportional to β^{-1}, controlled by $\epsilon_{ii}^{(2)}$, is responsible for shifting vibrational frequencies with cell volume, and as such is equivalent to classical Grüneisen theory for thermal expansion. The remaining terms generalize classical Grüneisen theory for complex nanostructures that involve coupling between vibrations and strain.

E. Analysis of the coupling

As we shall show below, it turns out that most of the L_i couplings vanish. The nonvanishing couplings still exert strong effects on bulk moduli and thermal expansion coefficients. Nonetheless, the fact that most couplings vanish is important for both computational efficiency and conceptual understanding. With relatively few couplings to compute, our theory can be parametrized from a tractably small number of density functional theory calculations. Moreover, insights into the compression and expansion of complex materials may be gleaned by visualizing the small number of vibrations that actually couple to strain. Before describing the computational methods used to parametrize our theory, we pause to reflect on why most of the couplings vanish.

This result follows from crystallographic symmetries and the stability of a given phase with respect to small lattice deformations. To elaborate on this, we start with a minimum energy ($T = 0$ K) structure. Next, we assume phase stability so that the space group symmetry of a given phase is conserved even if the lattice is deformed by a small strain δl. We further impose the constraint that the deformation δl conserves the unit cell shape. Using Eq. (1), we calculate the force per normal mode in the deformed configuration as

$$\frac{\partial E}{\partial x_i} = L_i\, \delta l + \mathcal{O}(x_i). \tag{31}$$

For the phase to be stable at $T = 0$ K, this force must vanish unless the normal mode x_i conserves the space group symmetry. Otherwise, the respective L_i must also vanish! This relatively strong condition causes most of the L_i couplings to vanish. For example, in fcc and bcc metals, all such couplings vanish and the thermal expansion comes only from the $\epsilon^{(0)} l^3$ anharmonicity and the frequency shift with volume as controlled by $\epsilon^{(2)} x^2 l$ terms. For such systems, the classical limit of Grüneisen theory is applicable. However, in zeolites and other complex nanostructures, which exhibit anharmonic modes coupled to lattice strain, these additional terms may have nontrivial and rather interesting contributions.

III. COMPUTATIONAL METHODS

Here we describe the density functional theory calculations we have performed to both parametrize and test the normal mode theory. We then discuss the spring-tetrahedron model used to generate normal modes of silica polymorphs.

A. Density functional theory calculations

We have performed density functional theory (DFT) calculations using plane wave basis sets, pseudopotentials, and

periodic supercells[20] as implemented in the Vienna Ab-Initio Simulation Package (VASP).[21–23] We used the local density approximation (LDA) of electron exchange-correlation based on Ceperley–Alder data.[24] In previous work, we[5,25] and others[26,27] have shown that LDA reproduces unit cell structures and volumes of silica polymorphs with surprising accuracy. Ion cores were represented by Vanderbilt-type ultrasoft pseudopotentials available within VASP.[28,29] Convergence tests were performed (data not shown) to ensure sufficient completeness of Brillouin zone sampling and plane wave basis sets. Below we give the results of these convergence tests for each system studied. To reduce the computer time, each structure was constrained to its putative space group symmetry during DFT calculations.

We have used DFT to analyze the normal modes of α-cristobalite, silica sodalite zeolite (Si-SOD) and an aluminosilica sodalite (Al-SOD). The sudden elastic force constants of silica zeolite structures CHA, LTA, and MOR[30] have also been computed with DFT. As a simple test of our anharmonic theory, the thermal expansion of fcc Al metal was studied. And finally, we have used DFT to parametrize our theory for the thermal expansion of Al-SOD.

1. α-Cristobalite, silica SOD, and aluminosilica SOD

We studied α-cristobalite because of ample experimental data on its bulk modulus,[31,32] and because its tetragonal lattice provides a good test of our theory for anisotropic solids. Our interest in Si-SOD was motivated by our recently reported DFT calculations finding that Si-SOD's bulk modulus is extremely sensitive to symmetry constraints.[5] Also, Al-SOD provides a good test of our anharmonic theory because of experimental thermal expansion data on the composition $Na_8Al_6Si_6O_{24}Cl_2$.[33,34]

α-cristobalite has a tetragonal unit cell, while Si-SOD and Al-SOD both exhibit cubic unit cells. We studied $I\,\bar{4}\,3\,m$ and $I\,m\,\bar{3}\,m$ symmetries of Si-SOD. The transition between the two phases was the subject of an earlier periodic DFT study.[35] In our DFT calculations, the latter is a saddle point on the potential energy surface, unstable at $T=0$ K. We found in our previous study that the bulk moduli for these phases are 18 and 93 GPa, respectively.[5] Below, we elucidate this remarkable sensitivity of the bulk modulus to symmetry constraints with our normal mode theory. We studied the $P\,\bar{4}\,3\,n$ symmetry of Al-SOD. The composition $Na_8Al_6Si_6O_{24}Cl_2$ of this Al-SOD features a highly symmetric arrangement of Na and Cl counterions.[33,34] The symmetry of α-cristobalite was constrained to $P\,4_1\,2_1\,2$.

The Brillouin zone was sampled using $2\times2\times2$ Monkhorst–Pack grids for the sodalites, and by using a $3\times3\times2$ grid for α-cristobalite.[36] For the sodalites, a plane wave cutoff of 420 eV was used, while for α-cristobalite, a cutoff of 460 eV was used to reduce noise in the total energy due to small energy differences.

As discussed above, the constants L_i vanish for normal mode displacements that break a given space group symmetry. Symmetry constraints can thus be used to dramatically reduce the number of coupled modes that need to be considered. We note that this reduction does not necessarily hold if lattice distortions become large enough so that anharmonicity with respect to lattice parameters, or symmetry-breaking unit cell deformations become important. The $I\,m\,\bar{3}\,m$ and $I\,\bar{4}\,3\,m$ symmetries of Si-SOD allow one and two coupled vibrations, respectively. The $P\,\bar{4}\,3\,n$ symmetry of Al-SOD gives four coupled vibrations, the two additional modes coming from counterion motion and Si–O–Al bond asymmetry.

To test our normal mode theory for the bulk modulus, we calculated the bulk moduli of α-cristobalite, Si-SOD, and Al-SOD using the conventional technique of varying unit cell volume, relaxing atomic coordinates, and fitting elements of the elastic tensor to the resulting energies as outlined in Ref. 5. In what follows, we denote these bulk moduli as B_{dir} because they arise directly from DFT-based optimizations, in contrast with the bulk moduli B_{theo}, which are computed with our normal mode theory through Eqs. (7) and (12). We used DFT to calculate direct bulk moduli of α-cristobalite, Si-SOD, and Al-SOD. Below we discuss a spring-tetrahedron model, from which direct and theoretical bulk moduli were also computed for various silica polymorphs.

2. Silica zeolites CHA, LTA, and MOR

We used DFT to calculate the force constants K (or $K_{jj'}$) for silica zeolite structures CHA, LTA, and MOR,[30] to compare their sudden elastic responses. We imposed the following space group symmetries for CHA, $R\,\bar{3}\,2/m$; for LTA, $P\,m\,\bar{3}\,m$; for MOR, $Cmcm$. These calculations were performed using a plane wave cutoff of 420 eV. For CHA and LTA, we used a $2\times2\times2$ Monkhorst–Pack grid, while for MOR we used a $1\times1\times2$ grid. High-silica LTA, which has recently been synthesized,[37] has a cubic structure, and hence has only one independent lattice parameter and force constant K. With rhombohedral CHA, we assumed that the lattice vector angle γ does not change. This is a reasonable assumption since γ has an equilibrium value close to 90° (94°), which does not change significantly as the volume is varied.[5] With orthorhombic MOR, we made an isotropic assumption, i.e., that the lattice parameters change uniformly and that the sudden elastic response is described by a single parameter K. This was necessary because of the computational expense of these DFT calculations.

3. Calibrating anharmonic theory with fcc Al metal

As a simple test of our anharmonic theory, we computed the thermal expansion coefficient of fcc Al metal. For the monatomic fcc lattice, none of the internal degrees of freedom is coupled to strain, and hence all the $L_i/2D_i$-type terms in Eq. (30) vanish. As such, we are left with the $\boldsymbol{\epsilon}^{(0)}$ and $\Sigma_i \epsilon_{ii}^{(2)}/D_i$ terms. These were calculated by varying the lattice parameter and estimating the force constant matrix for different values of l. Because all atoms in this structure are equivalent, and the structure is isotropic, the force constant matrix can be determined by displacing just a single atom in one Cartesian direction and computing the Hellmann–Feynman forces. System size effects were determined by comparing results from supercells containing 4 and 32 at-

oms, to check convergence with respect to the wavelength cutoff for normal modes. With the smaller cell, a $6\times6\times6$ Monkhorst-Pack grid was used, while with the larger cell a $4\times4\times4$ grid was sufficient. We found essentially identical results from these two system sizes, suggesting a minimal influence from system size effects. Because the ultrasoft pseudopotential for Al is significantly softer than that for oxygen, the plane wave cutoff can be reduced to 140 eV. The partial occupancies of Kohn-Sham eigenstates were treated by using a Gaussian smearing of 0.05 eV.

4. Parametrizing normal modes

The sudden elastic force constants K were computed by performing a series of DFT calculations on isotropically expanded and contracted solids. Polynomials were then fitted to the energies obtained. We calculated the force constants D_i by first computing elements of the nondiagonal force constant matrix, D'_{ij}, in some convenient representation. This was achieved by displacing atoms by small amounts, and calculating the resulting Hellmann-Feynman forces. A practical way to generate displacements consistent with symmetry is to vary the Wyckoff special positions of atoms.[2] The nondiagonal force constant matrix is then computed from the relation

$$F_i = -2\sum_j D'_{ij}q_j, \tag{32}$$

where F_i is the Hellmann-Feynman force, and $\{q_j\}$ are Cartesian atomic displacements. By diagonalizing $\mathbf{D}'$, we obtain the normal modes $\mathbf{x}$ and force constants $\{D_i\}$. The coupling constants L_i were obtained by simultaneously varying the lattice parameter and displacing atoms along normal mode directions, and fitting a polynomial to the resulting DFT energies.

In the $I\bar{4}3m$ phase of Si-SOD, O atoms occupy (x,x,y)-type Wyckoff special positions while Si atoms are located at (0.25, 0.5, 0.0)-type positions. As such, there are two internal degrees of freedom for this symmetry. The nondiagonal force constant matrix is calculated by making small displacements of O atoms of type $(\Delta,\Delta,0)$ and $(0,0,\Delta)$. We found that stable convergence is obtained for these force constants using $\Delta=10^{-2}$ Å. Diagonalizing the force constant matrix leads to two normal modes: one associated with relative rotations of several SiO_4 tetrahedra, and one with SiO_4 unit deformation. We thus expect the force constants for these normal modes to be significantly different. In the $Im\bar{3}m$ phase of Si-SOD, O atoms occupy $(x,x,0.5)$-type positions, thus giving only one internal degree of freedom, which turns out to be associated with SiO_4 unit deformation. The fact that relative rotations of SiO_4 tetrahedra are symmetry forbidden in the $Im\bar{3}m$ phase of Si-SOD already explains qualitatively why its bulk modulus is more than five times higher than that of $I\bar{4}3m$ Si-SOD.[5] Below we show that our normal mode theory accounts for this fact semiquantitatively as well.

In Al-SOD, Cl atoms are at (0,0,0)-type positions, Na at (u,u,u), Al at (0.25, 0.5, 0), Si at (0.25, 0, 0.5), and O at (x,y,z). As such, this symmetry allows four coupled internal degrees of freedom. The anharmonic terms were calculated as follows. Anharmonic constants for coupled modes were obtained by simultaneously displacing the lattice parameter and normal modes, and fitting the energies to a multivariable polynomial using least squares. The anharmonicities in $\Sigma_i\epsilon^{(2)}_{ii}/D_i$ and $L_j/2D_j\Sigma_i\epsilon^{(3)}_{iij}/D_i$ are less convenient to evaluate, because they require repeated calculations of the force constant matrix: for different values of the lattice parameter, and for displacements along the mode x_j, respectively. Fortunately, Al-SOD possesses enough symmetry to make several force constants interdependent. The full force constant matrix was evaluated with these symmetry properties as follows. We made $(\Delta,0,0)$ displacements for a single Na and a single Cl atom; we made $(\Delta,0,0)$, $(0,\Delta,0)$, and $(0,0,\Delta)$ displacements for a single Al, Si, and O atom. These calculations suffice to construct the full force constant matrix, because all atoms in a given sublattice are symmetry equivalent and the structure is isotropic.

In α-cristobalite, Si atoms are at $(u,u,0)$ positions while O atoms are at (x,y,z). As such, there are four internal degrees of freedom. The tetragonal unit cell has two independent lattice parameters. The coupling terms were calculated by making small displacements of the ith normal mode, and varying either the a lattice parameter, yielding L_{i1}-type terms, or the c parameter, yielding L_{i2}-type terms. The terms K_{11}, K_{12}, and K_{22} were calculated by varying the a and/or c lattice parameters while keeping atomic fractional coordinates fixed.

B. Spring-tetrahedron model

One difficulty with computing the normal modes of silica polymorphs with DFT is its high computational cost. This is especially true when one wishes to relax symmetry constraints. It is therefore worthwhile to pursue a simpler method that still captures the essential physics of elastic response in silica materials. Here we present such a model, based on semirigid SiO_4 tetrahedra connected with flexible springs. We show that this "spring-tetrahedron" model can indeed reproduce the elastic properties of a variety of silica polymorphs. We used this method to study the normal modes and bulk moduli of silica zeolites SOD, CHA, and LTA.[30] The bulk modulus and orthorhombic-to-low symmetry phase transition of silica MFI was also studied.

As discussed in the Introduction, our approach was inspired by rigid-unit models developed by Dove and coworkers to study soft vibrational modes in silica.[10] From a topological perspective, silica polymorphs can be viewed as networks of corner-sharing SiO_4 tetrahedra. The rigid-unit model assumes rigid tetrahedra connected with two-body springs.[10] Using this rigid-unit approach, we have found that some silica polymorphs became unstable at nonzero pressures because of barrierless deformation pathways. Furthermore, the bulk moduli of some zeolites are significantly overestimated with this approach, and calculating full normal mode spectra becomes impossible because deforming tetrahedra is forbidden.

A simple remedy is to allow tetrahedra to become somewhat flexible using two-body springs, and to add a three-

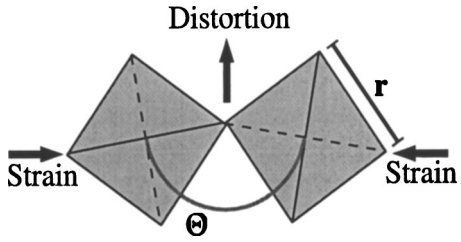

FIG. 1. A schematic showing the spring-tetrahedron system and its response to strain.

body term that penalizes the bending of Si-O-Si angles (Fig. 1), which we found restores mechanical stability. Although such an energy function with two-body and three-body springs begins to resemble valence bond force fields,[11,12] our approach is substantially different. Indeed, our spring-tetrahedron model only explicitly accounts for the positions of oxygen atoms in a given silica structure. For a unit cell with n_o oxygens, the spring-tetrahedron energy is given by

$$V(\mathbf{r}_1, \ldots, \mathbf{r}_{n_o}) = \frac{1}{2}\sum_{i=1}^{n_o}\sum_{k\in \mathrm{nn}_j}\frac{k_S}{2}(|\mathbf{r}_j - \mathbf{r}_k| - r_0)^2 + \sum_{i=1}^{n_o}\frac{k_A}{2}(\cos\theta_i - \cos\theta_0)^2, \qquad (33)$$

where $\mathbf{r}_j$ is the three-dimensional location of the jth oxygen, and "nn_j" are its six nearest neighbor oxygens. The factor of $\frac{1}{2}$ in the first term corrects for double counting. The parameter r_0 is the typical distance between oxygens in a given SiO_4 tetrahedron. The second term in Eq. (33) applies a spring to each Si-O_i-Si angle θ_i, i.e., to each shared vertex of adjacent tetrahedra (Fig. 1). Without explicit Si locations, we compute θ_i as the angle formed by the ith oxygen and the centers of mass of the two tetrahedra it joins. The spring-tetrahedron model thus replaces rigid tetrahedra with semirigid ones connected to each other by flexible springs, as controlled by the parameters $(k_S, k_A, r_0, \theta_0)$.

The spring-tetrahedron parameters were fitted to DFT-LDA data for Si-SOD ($I\bar{4}3m$), which serves as a bridge between dense and zeolitic silica polymorphs. The parameter r_0 contains much of the chemistry in Si-O bonding. Using a Si-O bond length of 1.6 Å and an O-Si-O bond angle of 109.47° gives $r_0 = \sqrt{8/3}\times 1.6$ Å $= 2.61$ Å. The reference Si-O-Si angle θ_0 was set to 155°, a value close to that found in Si-SOD ($I\bar{4}3m$), α-cristobalite, and in relaxed silica chain polymers.[25] The force constant k_S uniquely determines the sudden elastic response K, thereby allowing k_S to be fitted to the energy dependence of isotropic volume changes. The angular force constant k_A was fitted to the direct bulk modulus of Si-SOD ($I\bar{4}3m$) calculated from DFT-LDA data.[5] This was achieved by calculating the direct bulk modulus of Si-SOD using spring-tetrahedron potential energies, and varying k_A until this bulk modulus matched the DFT value.

We benchmarked the spring-tetrahedron model by calculating equilibrium volumes and bulk moduli of α-cristobalite and silica zeolite structures SOD, CHA, and LTA. In addition, we used the spring-tetrahedron model to generate the normal modes of SOD, CHA, and LTA, for use in decomposing their bulk moduli into sudden and vibrational contributions. These constitute predictions of properties that have not yet been measured. Unit cell shapes were held fixed during these calculations: tetragonal for α-cristobalite, cubic for SOD and LTA, and rhombohedral for CHA. No additional symmetry was imposed on atomic coordinates. To avoid a divergence when calculating terms of the form $L_i^2/4D_i$, we removed the three normal modes corresponding to the center-of-mass translation, whose normal force constants vanish.

To further test the spring-tetrahedron model, we computed the bulk modulus of silica MFI zeolite. With MFI, an additional complexity stems from a structural phase transition between monoclinic and orthorhombic phases.[38] Because our normal mode theory assumes that unit cell shapes remain preserved despite strains and vibrations, this theory cannot be applied to study the transition of MFI between different unit cell shapes. Instead, we performed direct optimizations to determine the bulk modulus. However, local optimization algorithms yielded unsatisfactory results because of a rugged energy landscape. As such, we annealed the structure using Metropolis Monte Carlo simulations.[39] The bulk modulus was extracted by adding a pV term to the energy, and mapping the equilibrium volume as a function of pressure. All internal coordinates and lattice vectors were allowed to vary. We show below that the spring-tetrahedron model exhibits a phase transition for MFI from orthorhombic to lower symmetry at small *negative* pressures.

IV. RESULTS

Here we present the numerical results of our study on the mechanical properties of nanostructured silica. We begin by comparing sudden elastic responses from various silica polymorphs calculated from DFT. We then present the best-fit parameters and predictions of the spring-tetrahedron model for a comparison with DFT data. Next we discuss the normal modes of Si-SOD generated by DFT and spring-tetrahedron energies, as well as the normal modes of Al-SOD and α-cristobalite obtained from DFT. We then apply the spring-tetrahedron model to explore the bulk moduli of CHA, LTA, and MFI zeolites. We close this section with the thermal expansion coefficients of fcc Al metal and Al-SOD zeolite computed from DFT.

A. Sudden elastic responses from DFT

Sudden elastic response constants computed from DFT for various silica polymorphs are shown in Table I. For cubic lattices, these are converted to units of GPa according to $B_{\mathrm{sud}} = (2/9a_0)K$. For noncubic lattices, B_{sud} is computed from Eq. (12) by setting the couplings L_{ij} to zero. The corresponding direct bulk moduli are also shown in Table I. While the bulk moduli in Table I show a significant variation from one polymorph to another, the sudden elastic response constants exhibit remarkable uniformity. Indeed, the spread in B_{dir} values amounts to 60% of its average, whereas that for B_{sud} is

TABLE I. Sudden elastic responses and direct bulk moduli (GPa) of various silica polymorphs computed with DFT. Sudden elastic responses given as $B_{sud}=(2/9a_0)K$ for cubic systems SOD and LTA. For anisotropic lattices α-cristobalite and CHA, B_{sud} is computed from Eq. (12) setting couplings L_{ij} to zero. For MOR, B_{sud} is approximated by changing the lattice parameters uniformly and assuming a scalar K.

	B_{sud}	B_{dir}
SOD $I\bar{4}3m$	118	18
SOD $Im\bar{3}m$	112	93
LTA	92	46
CHA	103	68
α-cristobalite	76	8
MOR	117	57

only 15%. This uniformity among sudden elastic responses reflects the intrinsic rigidity of SiO_4 tetrahedra shared by all silica polymorphs. The unformity of sudden elastic response constants is well reproduced by the spring-tetrahedron model.

B. Spring-tetrahedron model parameters

The spring-tetrahedron force constants k_S and k_A in Eq. (33) were fitted to the sudden elastic force constant and bulk modulus of Si-SOD ($I\bar{4}3m$). As shown in Table I, these take the values 118 and 18 GPa, respectively. The resulting best-fit parameters are given in Table II. To test the spring-tetrahedron model, we computed the bulk moduli and unit cell volumes of Si-SOD ($I\bar{4}3m$), CHA, LTA, and α-cristobalite. Table III shows the spring-tetrahedron results alongside the corresponding DFT data. The agreement is excellent, considering the simplicity of the spring-tetrahedron potential function. For the dense polymorph α-cristobalite, the unit cell volume agrees well while the bulk modulus is somewhat overestimated. Spring-tetrahedron energy differences between different silica polymorphs are small (data not shown), which is in qualitative agreement with experimental data[40] and DFT calculations.[5]

C. Normal modes of Si-SOD from DFT and the spring-tetrahedron model

The normal mode analyses of Si-SOD from DFT with lower symmetry ($I\bar{4}3m$) and higher symmetry ($Im\bar{3}m$) are presented in Table IV. Also shown in Table IV is the normal mode analysis of Si-SOD based on the spring-tetrahedron model with no imposed symmetry, which yields a pattern of couplings essentially identical to the DFT results for Si-SOD ($I\bar{4}3m$). An inspection of Table IV shows that the spring-tetrahedron model performs well in reproducing the results of DFT calculations. High symmetry Si-SOD exhibits a normal vibration corresponding to the deformation of individual SiO_4 tetrahedra, denoted mode 1. Low symmetry Si-SOD allows this mode as well as another, denoted mode 2, corresponding to rotations of adjacent SiO_4 tetrahedra relative to each other. These two vibrations are shown schematically in Fig. 2.

TABLE II. Parameters for the spring-tetrahedron model.

k_S	8.82 eV/Å^2
k_A	2.35 eV
r_0	2.61 Å
θ_0	155°

TABLE III. Direct bulk moduli (GPa) and equilibrium unit cell volumes (Å^3) computed using DFT and the spring-tetrahedron model (STM).

	B_{dir}, DFT	B_{dir}, STM	V_0, DFT	V_0, STM
SOD $I\bar{4}3m$	18	18	57	57
CHA	68	67	65	66
LTA	46	54	69	70
α-cristobalite	8	13	46	44

The sudden elastic response constants of the two symmetries of Si-SOD are quite similar, as discussed above. The extent to which the bulk modulus is decreased from mode 1 is also quite similar between the forms of Si-SOD, as demonstrated by the values of $L_1^2/4D_1$ in Table IV. However, because mode 2 involves relative rotations of SiO_4 tetrahedra, the force constant D_2 is much smaller than D_1, leading to a much greater diminution of the bulk modulus from mode 2 in Si-SOD ($I\bar{4}3m$). This explains why the bulk moduli are so different, even though these two forms of Si-SOD have nearly identical atomic configurations.

TABLE IV. Sudden elastic responses and vibrational coupling terms (GPa) for two symmetries of Si-SOD, from DFT and the spring-tetrahedron model (STM). High symmetry ($Im\bar{3}m$) STM calculations were not performed. Results are multiplied by $2/9a_0$ to obtain GPa units. Direct and theoretical bulk moduli, B_{dir} and B_{theo}, are also shown for comparison.

Si-SOD $I\bar{4}3m$	DFT	STM
K	118	112
$L_1^2/4D_1$	16	14
$L_2^2/4D_2$	79	80
B_{theo}	23	18
B_{dir}	18	18
Si-SOD $Im\bar{3}m$	**DFT**	
K	112	
$L_1^2/4D_1$	14	
B_{theo}	98	
B_{dir}	93	

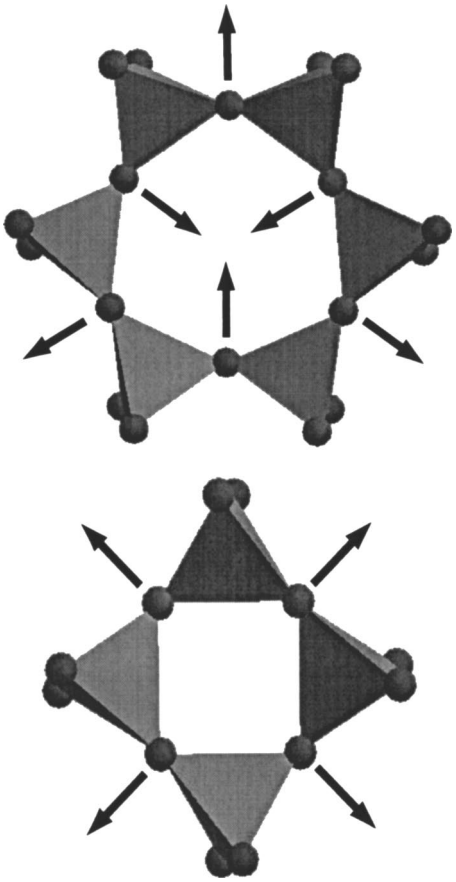

FIG. 2. Schematic representation of the soft (up) and hard (down) normal modes in Si-SOD, in which tetrahedra represent SiO_4 units. In the upper picture the six ring is viewed along the [111] axis, while in the lower picture the four ring is viewed down the [100] axis. Normal mode displacement vectors are projected onto corresponding planes.

Also shown in Table IV are bulk moduli computed from direct optimizations and normal mode theory. These are in excellent agreement, signaling the first numerical success of our normal mode theory of elastic response.

D. Normal modes of Al-SOD and α-cristobalite from DFT

The normal mode analysis of Al-SOD ($Na_8Al_6Si_6O_{24}Cl_2$) from DFT is presented in Table V. Due to the presence of Al and counterions in the structure, the couplings in Al-SOD are split into four vibrations coupled to strain. As with the other solids discussed above, the sudden elastic response constant for Al-SOD is near 100 GPa. Normal vibrations 1 and 3 decrease the bulk modulus by about 40%, with another 10% decrease coming from vibrations 2 and 4.

TABLE V. Sudden elastic response and vibrational coupling terms (GPa) for Al-SOD from DFT. Results are multiplied by $2/9a_0$ to obtain GPa units. The theoretical bulk modulus is also shown.

K	107
$L_1^2/4D_1$	20
$L_2^2/4D_2$	5
$L_3^2/4D_3$	23
$L_4^2/4D_4$	4
B_{theo}	55

TABLE VI. Sudden elastic force constants $K_{jj'}$ and coupling terms $L_{ij}L_{ij'}/4D_i$ (eV/Å^2) for α-cristobalite from DFT. Direct and theoretical bulk moduli, B_{dir} and B_{theo} in GPa, are also shown for comparison with experimental values B_{exp}.

K_{11}	14.936
K_{12}	3.699
K_{22}	3.360
$L_{11}^2/4D_1$	11.271
$L_{11}L_{12}/4D_1$	3.822
$L_{12}^2/4D_1$	1.292
$L_{21}^2/4D_2$	0.210
$L_{21}L_{22}/4D_2$	0.125
$L_{22}^2/4D_2$	0.074
$L_{31}^2/4D_3$	0.595
$L_{31}L_{32}/4D_3$	0.514
$L_{32}^2/4D_3$	0.382
$L_{41}^2/4D_4$	0.784
$L_{41}L_{42}/4D_4$	−0.708
$L_{42}^2/4D_4$	0.640
B_{theo}	11
B_{dir}	8
B_{exp} (Ref. 31)	16.0
B_{exp} (Ref. 32)	11.5

In contrast to Si-SOD, Al-SOD exhibits stronger mixing between deformations and relative rotations of tetrahedra. In the softest mode (mode 1), the motion of framework O atoms and Na counterions is in phase, while in the next more rigid mode (mode 2) they are in antiphase. The third softest mode (mode 3) consists of a mixture of rotations and deformations, while the fourth and most rigid mode (mode 4) has a strong component of O atom displacement along the Si−Al internuclear axis. These modes couple to strain in such a way that modes 1 and 3 exert the greatest diminution on the bulk modulus. In contrast to Si-SOD, none of these modes is very soft, leading to a bulk modulus of 55 GPa. This likely arises from counterions in Al-SOD stiffening of the relative rotations of SiO_4 tetrahedra.

Studying α-cristobalite allows us to test our normal mode theory on an anisotropic structure. However, the effects of individual modes on the bulk modulus is blurred because the matrix inverse in Eq. (12) mixes the terms $L_{ij}L_{ij'}/4D_i$ among the coupled modes $i=1,\ldots,4$. Due to the tetragonal unit cell of α-cristobalite, varying the lattice parameter a requires changing b by the same amount. The total effect on the unit cell volume is greater compared to that from varying c alone, making the force constants associated with the lattice parameter a larger. As shown in Table VI, the $L_{ij}L_{ij'}/4D_i$ terms for the softest mode (mode 1) are again the largest. This mode

TABLE VII. Sudden elastic force constants and coupling terms (GPa) for silica CHA from the spring-tetrahedron model (STM). Each term is converted to GPa units using Eq. (12), setting either $K'=K$ or $K'=L_i^2/4D_i$, and setting all other terms to zero. Direct and theoretical bulk moduli from STM potential energies are also shown for a comparison.

K	97
$L_1^2/4D_1$	2
$L_2^2/4D_2$	2
$L_3^2/4D_3$	1
$L_4^2/4D_4$	8
$L_5^2/4D_5$	1
$L_6^2/4D_6$	16
B_{theo}	67
B_{dir}	67

consists mostly of rigid-body rotations and translations of SiO_4 tetrahedra. The remaining three modes consist of SiO_4 tetrahedral deformations of increasing magnitude from modes 2 to 4.

Also shown in Table VI are the direct and normal mode bulk moduli of α-cristobalite from DFT. These are 8 and 11 GPa, respectively, diminished from a sudden elastic response of 76 GPa. Experimental values of α-cristobalite's bulk modulus are 16.0 GPa[31] and 11.5 GPa,[32] which are in reasonable agreement with our direct and theoretical results, considering the spread in experimental values. This level of agreement bodes well for our normal mode theory of anisotropic lattices.

E. Normal modes of CHA and LTA from the spring-tetrahedron model

The normal modes of silica zeolite structures SOD, CHA, and LTA were analyzed with the spring-tetrahedron model by keeping the respective unit cell shapes fixed, but without additional symmetry constraints. Despite this relaxation of symmetry, most of the L_i couplings were still found to vanish. This is expected to occur for crystal structures whose symmetry is nearly preserved by the spring-tetrahedron model, because the symmetric structure is close to a local minimum of the spring-tetrahedron potential. Such a result was found above for Si-SOD ($I\,\bar{4}\,3\,m$), but would not be expected for the higher symmetry $I\,m\,\bar{3}\,m$ structure, because this is a saddle point of the spring-tetrahedron potential.[5]

The spring-tetrahedron model applied to CHA predicts that six vibrations are coupled to lattice strain, as shown in Table VII. Starting with a sudden elastic response constant of 97 GPa, only two modes significantly influence the elastic response. When applied to LTA, the spring-tetrahedron model identifies four modes coupled to strain. Each of these modes diminishes the bulk modulus significantly from its sudden elastic value of 92 GPa, as shown in Table VIII. It is remarkable that, even though SOD and LTA are both built from SOD cages, the elastic response of LTA is not softened by vibrations as much as was found for Si-SOD ($I\,\bar{4}\,3\,m$) (see Table IV). The direct and normal mode bulk moduli of CHA and LTA are in perfect agreement, which might be expected when applying a harmonic theory to a spring potential.

TABLE VIII. Sudden elastic force constants and coupling terms (GPa) for silica LTA from the spring-tetrahedron model (STM). Results are multiplied by $2/9a_0$ to obtain GPa units. Direct and theoretical bulk moduli from STM potential energies, B_{dir} and B_{theo}, are also shown for comparison.

K	92
$L_1^2/4D_1$	14
$L_2^2/4D_2$	8
$L_3^2/4D_3$	5
$L_4^2/4D_4$	11
B_{theo}	54
B_{dir}	54

F. Mechanical properties of MFI from the spring-tetrahedron model

We investigated the applicability of the spring-tetrahedron model to study the elastic properties and phase behavior of silica MFI (silicalite). We annealed the structure at various pressures to obtain the $T=0$ K equilibrium volume as a function of pressure. The behavior of the unit cell volume versus pressure is shown in Fig. 3. Under compression at positive pressures, the bulk modulus takes the value 12–13 GPa. A unit cell slightly distorted from an orthorhombic shape is obtained. Due to very small distortions in the lattice vector angles, the exact symmetry of this phase is difficult to identify. We also considered the hypothetical possibility of negative pressures, i.e., when the structure is under tension. Such a situation may effectively occur when the lattice is loaded with guest molecules, which pull inward into the pores through host–guest attractions. In this case the bulk modulus takes the value 65 ± 5 GPa. At the transition point the unit cell deforms from orthorhombic to a lower symmetry phase.

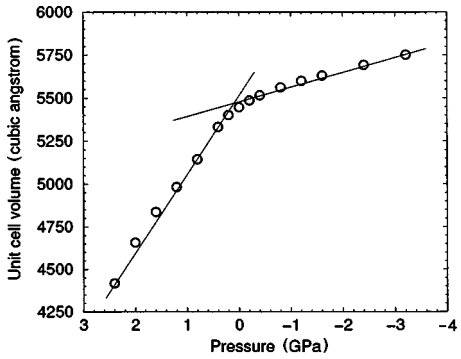

FIG. 3. Behavior of the unit cell volume of Si-MFI as the structure is annealed at different pressures. The two lines highlight the transition from low symmetry to an orthorhombic structure.

Our previous DFT study on orthorhombic MFI gave a bulk modulus of 41 GPa.[5] Although the predictions of the spring-tetrahedron model are not too far from this value, a much more careful analysis is required before the elastic properties and phase behavior of MFI are well understood.

G. Thermal expansion of fcc Al metal from DFT

We now turn our attention to the thermal expansion coefficient, beginning with a test of our theory on fcc Al metal with parameters computed by DFT. We first calibrate the accuracy of DFT-LDA with ultrasoft pseudopotentials for fcc Al, by discussing its lattice parameter and bulk modulus. Our calculated lattice parameter is 3.98 Å, which is in good agreement with the experimental room temperature value of 4.05 Å, and in excellent agreement with a previous DFT-LDA result of 3.97 Å obtained with norm-conserving pseudopotentials.[41,42] Our calculated bulk modulus for fcc Al with a 4-atom unit cell is 84 GPa; with a 32-atom unit cell we obtain 81 GPa. This agrees well with the experimental value of 75.9 GPa, and with the previous DFT-LDA value of 79.4 GPa.[41,42]

We obtain a thermal expansion coefficient $C=62\times10^{-6}\ \mathrm{K}^{-1}$ for fcc Al using a 4-atom supercell. This agrees well with the experimental room-temperature value of $65\times10^{-6}\ \mathrm{K}^{-1}$, and with earlier DFT results based on Debye-Grüneisen theory.[9,42] Effects from quantized vibrations are negligible at room temperature for fcc Al, because the thermal expansion coefficient and specific heat have already reached plateaus at this temperature. Using the 32-atom supercell, we obtain a value of $67\times10^{-6}\ \mathrm{K}^{-1}$, indicating that convergence with respect to normal mode wavelength cutoff has been reached. With the smaller supercell, more than 90% of the thermal expansion coefficient stems from the $\Sigma_i^n \epsilon_{ii}^{(2)}/D_i$ term. In the case of the larger supercell, this term contributes more than 99%, confirming the scaling behavior discussed above for Eq. (30).

H. Thermal Expansion of Al-SOD from DFT

To explore how coupling between vibrations and strain influences thermal expansion, we now consider Al-SOD ($Na_8Al_6Si_6O_{24}Cl_2$) with anharmonicities computed from DFT. Though in principle the thermal expansion of Al-SOD depends on several anharmonic terms, in practice the greatest contributions come from terms of the form $\Sigma_i^n \epsilon_{ii}^{(2)}/D_i$ and $\Sigma_{ij}^n (L_j/2D_j)\epsilon_{iij}^{(3)}/D_i$ in Eq. (30). In the temperature range 250–750 K, very good agreement with experimental volume data is seen in Fig. 4. Our calculated value of the thermal expansion coefficient is $37\times10^{-6}\ \mathrm{K}^{-1}$, which compares well with the experimental values at 500 K of $39.5\times10^{-6}\ \mathrm{K}^{-1}$,[33] and $33.9\times10^{-6}\ \mathrm{K}^{-1}$.[34] The systematic underestimation of equilibrium volume by 3–4% evident in Fig. 4 is characteristic of the LDA functional.

We have not systematically tested the convergence with respect to system size for Al-SOD, and therefore should put fairly large error bars on these thermal expansion results. Additional calculations with larger Al-SOD systems would be nearly computationally impossible at present, because the next bigger cubic cell for Al-SOD contains over 300 atoms. However, a reasonably converged result for Al metal was obtained using a supercell that is much smaller than the one for Al-SOD, suggesting that our results for Al-SOD are likely valid. In addition, the fact that our thermal expansion results for Al-SOD agree well with experiments further suggests that the accuracy of our computations has not been compromised by finite size effects.

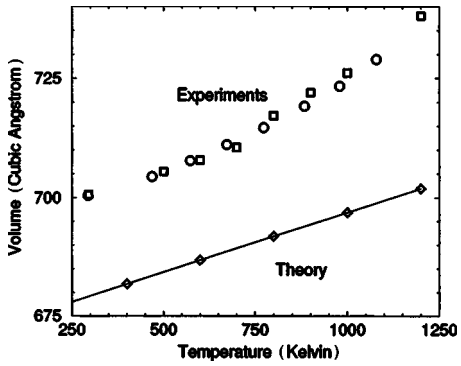

FIG. 4. Comparing experimental and theoretical data on the temperature dependence of Al-SOD unit cell volume. Experimental points are circles (Ref. 33) and squares (Ref. 34). Theoretical points are computed from Eq. (30) parametrized by DFT.

We note that only about $8\times10^{-6}\ \mathrm{K}^{-1}$ of the thermal expansion coefficient stems from the term $\Sigma_i \epsilon_{ii}^{(2)}/D_i$, while $\Sigma_{ij}^n (L_j/2D_j)\epsilon_{iij}^{(3)}/D_i$ accounts for the remaining $29\times10^{-6}\ \mathrm{K}^{-1}$. This suggests that Grüneisen theory would only account for 22% of the thermal expansion coefficient of Al-SOD, because it ignores the coupling between strain and anharmonic vibrations.

V. DISCUSSION AND CONCLUDING REMARKS

We have presented a method for analyzing the mechanical properties of solids, based on normal modes and their coupling to lattice strains. This method was used to study elastic compression and thermal expansion of silica zeolites and related materials, with parameters calculated from density functional theory (DFT) calculations. We have found in general that the bulk modulus can be divided into two contributions: a positive term arising from compression without internal relaxation, which we call the sudden elastic response, and a negative term from coupling between compression and internal vibrational modes. For silica polymorphs, the sudden elastic response term varies little among the phases studied, taking values near 100 GPa because of the intrinsic rigidity of SiO_4 tetrahedra. In contrast, the latter term varies strongly from one polymorph to the next, because each polymorph exhibits different symmetry constraints on internal vibrations and their couplings to lattice strains. Numerical results of this approach agree well with experiment for the dense silica polymorph α-cristobalite. The normal mode theory gives results that agree well with previous DFT calculations for silica zeolite structures SOD, CHA, and LTA. We hope that these developments will spawn new experiments to test our predictions on the mechanical properties of nanostructured silica.

We have found that, for a given structure, only a few normal modes influence the bulk modulus. This follows from crystallographic symmetries and the stability of a given phase with respect to small lattice deformations. The modes that do couple exert strong effects on bulk moduli and thermal expansion coefficients. Nonetheless, the fact that most couplings vanish is important for both computational efficiency and conceptual understanding. With relatively few couplings to compute, our theory can be parametrized from a tractably small number of DFT calculations. In addition, insights into the compression and expansion of complex materials may be gleaned by visualizing the small number of vibrations that actually couple to strain.

When comparing the properties of normal modes in Si-SOD and Al-SOD, we found that the more complex chemical composition, i.e., going from Si-O to Si-O-Al-Na-Cl, tends to mix the vibrations. The presence of ionized species Na and Cl appears to stiffen the vibrations. For a given composition, structures with lower symmetry generally permit a larger number of coupled modes, but in such structures the mixing between soft Si-O-Si bending modes and hard O-Si-O bend and Si-O stretch modes may reduce the effect of such couplings.

We augmented our harmonic theory with a perturbative treatment of anharmonic terms, allowing the calculation of the thermal expansion coefficient. The resulting expression provides a generalization of classical Grüneisen theory, wherein phonon frequencies are calculated at different volumes to obtain the free energy as a function of volume. We found that Grüneisen theory ignores bilinear couplings between lattice strain and anharmonic vibrations. We have applied our approach to the thermal expansion of fcc aluminum metal and an aluminosilica sodalite zeolite. In the former case, we found that our theory reproduces the success of classical Grüneisen theory. In the latter case, our approach gives excellent agreement with experiment, while Grüneisen theory accounts for only 22% of the thermal expansion coefficient. This result shows that in general, including couplings between vibrations and strain will be important for predictive models of thermal expansion.

To facilitate the parametrization of this normal mode model, we constructed a simplified classical spring-tetrahedron model for silica. This is especially useful when one wishes to relax symmetry constraints. Our spring-tetrahedron model is based on semirigid SiO_4 tetrahedra connected with flexible springs. After fitting to properties of silica sodalite determined from DFT, this model reproduces experimental cell volumes and predicts bulk moduli of α-cristobalite and silica zeolites CHA, LTA, and MFI. The spring-tetrahedron model also captures the fact that the sudden elastic response varies little from one silica polymorph to the next.

The spring-tetrahedron model was used to analyze the normal modes of silica zeolite structures SOD, CHA, and LTA. When comparing with DFT calculations on SOD, we found that the spring-tetrahedron model generates the correct normal modes, and perhaps more remarkably, the model quantitatively reproduces the couplings of these modes to lattice strain. We have found that silica polymorphs can be divided in two categories: structures that allow low-frequency vibrations to soften the elastic response (e.g., α-cristobalite and SOD), and materials with network and symmetry constraints that preclude such softening (e.g., CHA and LTA). When applying the spring-tetrahedron model to silica MFI zeolite, we observed a transition between these two regimes involving a transformation from low-symmetry to an orthorhombic phase.

In the end we find that the normal mode picture of compression and expansion, parametrized by DFT calculations and the spring-tetrahedron model, provides a powerful new approach for understanding the mechanical properties of nanostructured materials. Despite this progress, much future work is suggested by the present study. We plan to develop the theory of thermal expansion for anisotropic solids. We will also pursue a quantum version of our normal mode theory. Treating strain as a slow mode within the adiabatic approximation should yield a simple theory for the bulk modulus. However, developing a quantum theory for thermal expansion remains quite challenging. Finally, we plan to study the phase transition observed in MFI in more detail to determine the connection between our calculations and experimental data.

Note added in proof. Equation (7) also shows that our theory predicts a bulk modulus that does not depend on temperature. Even when accounting for anisotropy and anharmonicity, the resulting formulas for the bulk modulus do not depend on temperature either. Experimental data for bulk moduli often exhibit very weak temperature dependencies. Indeed, over the temperature range 300–1800 K, bulk moduli of α-Al_2O_3 and SiC only change by 12.5% and 9.4%, respectively.[43]

ACKNOWLEDGMENTS

The authors thank the National Science Foundation for their generous support through a Nanoscale Interdisciplinary Research Team (NIRT) grant (CTS-0103010).

APPENDIX: DERIVATION OF THE ANISOTROPIC BULK MODULUS, EQ. (12)

Beginning with Eq. (8), we write the equilibrium volume change singling out the nth normal mode according to

$$\begin{aligned}\langle \Delta V \rangle = & -\frac{\partial}{\beta \partial p} \ln \int_{-\infty}^{\infty} dx_1 \cdots dx_n \, dl_1 \cdots dl_m \\ & \times \exp\left\{ -\beta \left[\sum_{i=1}^{n-1} \left(D_i x_i^2 + \sum_{j=1}^{m} L_{ij} x_i l_j \right) \right.\right. \\ & \left.\left. + \sum_{j,j'=1}^{m} K_{jj'} l_j l_{j'} + p \sum_{j=1}^{m} c_j l_j \right] \right\} \\ & \times \exp\left\{ -\beta \left[\left(D_n x_n^2 + \sum_{j=1}^{m} L_{nj} x_n l_j \right) \right] \right\}. \end{aligned} \quad \text{(A1)}$$

After integrating out the nth normal mode we obtain

$$\langle \Delta V \rangle = -\frac{\partial}{\beta \partial p} \ln \int_{-\infty}^{\infty} dx_1 \cdots dx_{n-1}\, dl_1 \cdots dl_m \times \exp\left\{ -\beta \left[\sum_{i=1}^{n-1} \left(D_i x_i^2 + \sum_{j=1}^{m} L_{ij} x_i l_j \right) + \sum_{j,j'=1}^{m} K_{jj'} l_j l_{j'} + p \sum_{j=1}^{m} c_j l_j \right] \right\} \exp\left[(\beta/4D_n) \left(\sum_{j=1}^{m} L_{nj} l_j \right)^2 \right]. \quad \text{(A2)}$$

In a fashion analogous to the cubic case, coupling to mode n effectively reduces the sudden elastice force constants from $K_{jj'}$ to $K_{jj'} - L_{nj} L_{nj'}/4D_n$. However, in the anisotropic case the L_{nj} couplings become mixed. After integrating over the remaining normal modes, we obtain

$$\langle \Delta V \rangle = -\frac{\partial}{\beta \partial p} \ln \int_{-\infty}^{\infty} dl_1 \cdots dl_m \times \exp\left[-\beta \left(\sum_{j,j'=1}^{m} K'_{jj'} l_j l_{j'} + p \sum_{j=1}^{m} c_j l_j \right) \right], \quad \text{(A3)}$$

where

$$K'_{jj'} = K_{jj'} - \sum_{i=1}^{n} \frac{L_{ij} L_{ij'}}{4D_i}. \quad \text{(A4)}$$

This can be evaluated using standard techniques of multidimensional Gaussian integration, yielding

$$\langle \Delta V \rangle = -\frac{\partial}{\beta \partial p} \ln \exp\left[\frac{\beta p^2}{4} (\mathbf{c}^T \mathbf{K}'^{-1} \mathbf{c}) \right]. \quad \text{(A5)}$$

By taking the derivatives and inserting the result into Eq. (2), we obtain Eq. (12).

*Electronic address: astala@ecs.umass.edu
†Electronic address: auerbach@chem.umass.edu
‡Electronic address: monson@ecs.umass.edu

[1] T. J. Barton, L. M. Bull, W. G. Klemperer, D. A. Loy, B. McEnaney, M. Misono, P. A. Monson, G. Pez, G. W. Scherer, J. C. Vartuli *et al.*, Chem. Mater. **11**, 2633 (1999).
[2] R. Wyckoff, *Crystal Structures Volume 2* (Interscience, New York, 1965).
[3] S. M. Auerbach, K. A. Carrado, and P. K. Dutta, eds., *Handbook of Zeolite Science and Technology* (Marcel Dekker, Inc., New York, 2003).
[4] M. H. Ford, S. M. Auerbach, and P. A. Monson, J. Chem. Phys. **121**, 8415 (2004).
[5] R. Astala, S. M. Auerbach, and P. A. Monson, J. Phys. Chem. B **108**, 9208 (2004).
[6] L. J. Gibson and M. F. Ashby, *Cellular Solids: Structure and Properties* (Cambridge University Press, Cambridge, UK, 1997), 2nd ed.
[7] M. Born and H. Kun, *Dynamical Theory of Crystal Lattices* (Oxford University Press, Oxford, 1985).
[8] A. A. Maradudin, E. W. Montroll, and G. H. Weiss, *Theory of Lattice Dynamics in the Harmonic Approximation* (Academic Press Inc., London, 1963).
[9] Y. S. Touloukian, R. K. Kirby, R. E. Taylor, and P. D. Desai, *Thermophysical Properties of Matter, Volume 12, Thermal Expansion, Metallic Elements and Alloys* (IFI/Plenum, New York, 1975).
[10] K. D. Hammonds, V. Heine, and M. T. Dove, J. Phys. Chem. B **102**, 1759 (1998).
[11] P. Demontis and G. B. Suffritti, Chem. Rev. (Washington, D.C.) **97**, 2845 (1997).
[12] K. S. Smirnov and D. Bougeard, Catal. Today **70**, 243 (2001).
[13] E. Pollak, J. Chem. Phys. **85**, 865 (1986).
[14] M. E. Lines and A. M. Glass, *Principles and Applications of Ferroelectrics and Related Materials* (Oxford University Press, Chippenham, 1977).
[15] K. M. Rabe and J. D. Joannopoulos, Phys. Rev. Lett. **59**, 570 (1987).
[16] A. Garćia and D. Vanderbilt, Phys. Rev. B **54**, 3817 (1996).
[17] E. B. Wilson, Jr., J. C. Decius, and P. C. Cross, *Molecular Vibrations: The Theory of Infrared and Raman Vibrational Spectra* (McGraw-Hill, New York, 1955).
[18] D. A. Woodcock, P. Lightfoot, L. A. Villaescusa, M.-J. Díaz-Cabañas, M. A. Camblor, and D. Engberg, Chem. Mater. **11**, 2508 (1999).
[19] V. Heine, P. R. L. Welch, and M. T. Dove, J. Am. Ceram. Soc. **82**, 1793 (1999).
[20] M. C. Payne, M. P. Teter, D. C. Allan, T. A. Arias, and J. D. Joannapoulos, Rev. Mod. Phys. **64**, 1045 (1992).
[21] G. Kresse and J. Furthmüller, Phys. Rev. B **54**, 11 169 (1996).
[22] G. Kresse and J. Hafner, Phys. Rev. B **47**, 558 (1993).
[23] G. Kresse and J. Hafner, Phys. Rev. B **49**, 14 251 (1994).
[24] D. M. Ceperley and B. J. Alder, Phys. Rev. Lett. **45**, 566 (1980).
[25] R. Astala and S. M. Auerbach, J. Am. Chem. Soc. **126**, 1843 (2004).
[26] T. Demuth, Y. Jeanvoine, J. Hafner, and J. G. Ángyán, J. Phys.: Condens. Matter **11**, 3833 (1999).
[27] T. Demuth, J. Hafner, L. Benco, and H. Toulhoat, J. Phys. Chem. B **104**, 4593 (2000).
[28] D. Vanderbilt, Phys. Rev. B **41**, 7892 (1990).
[29] G. Kresse and J. Hafner, J. Phys.: Condens. Matter **6**, 8245 (1994).
[30] C. Baerlocher, W. M. Meier, and D. H. Olson, *Atlas of Zeolite Framework Types* (Elsevier, Amsterdam, 2001), 5th ed.
[31] A. Yeganeh-Haeri, D. J. Weidner, and J. B. Parise, Science **257**, 650 (1992).
[32] R. T. Downs and D. C. Palmer, Am. Mineral. **79**, 9 (1994).
[33] C. M. B. Henderson and D. Taylor, Phys. Chem. Miner. **2**, 337 (1978).
[34] R. K. McMullan, S. Ghose, N. Haga, and V. Schomaker, Acta Crystallogr., Sect. B: Struct. Sci. **52**, 616 (1996).
[35] K. Knorr, B. Winkler, and V. Milman, Z. Kristallogr. **216**, 495

(2001).
[36] H. J. Monkhorst and J. D. Pack, Phys. Rev. B **13**, 5188 (1974).
[37] A. Corma, F. Rey, J. Rius, M. J. Sabater, and S. Valencia, Nature (London) **431**, 287 (2004).
[38] E. L. Wu, S. L. Lawton, D. H. Olson, A. C. Rohrman, Jr., and G. T. Kokotailo, J. Phys. Chem. **83**, 2777 (1979).
[39] D. Frenkel and B. Smit, *Understanding Molecular Simulations* (Academic Press, San Diego, 1996).
[40] I. Petrovic, A. Navrotsky, M. E. Davis, and S. I. Zones, Chem. Mater. **5**, 1805 (1993).
[41] D. R. Lide, H. P. R. Fredrikse, and H. W. King, eds., *CRC Handbook of Chemistry and Physics* (CRC Press, Boca Raton, FL, 2003).
[42] A. Debernardi, M. Alouani, and H. Dreyssé, Phys. Rev. B **63**, 064305 (2001).
[43] K. Sivasubramanian, S. Raju, and E. Mohandas, J. Eur. Ceram. Soc. **21**, 1229 (2001).